

Electrochimica Acta

Electrochemical performance of Manganese Hexacyanoferrate cathode material in aqueous Zn-ion battery --Manuscript Draft--

Manuscript Number:	
Article Type:	VSI:EESC 2021
Keywords:	Sodium manganese hexacyanoferrate; Aqueous Zn-ion battery; Mn/Fe-site study; ex-situ XAS spectra
Corresponding Author:	Marco Giorgetti, Ph.D. University of Bologna Bologna, BO ITALY
First Author:	Min Li
Order of Authors:	Min Li Rosalinda Sciacca Mariam Maisuradze Giuliana Aquilanti Jasper Plaisier Mario Berrettoni Marco Giorgetti, Ph.D.
Abstract:	<p>Manganese hexacyanoferrate (MnHCF) has attracted much attention as promising cathode material for Li and Na ion batteries, owing to its low cost, environmental friendliness, high specific capacity and voltage plateau. Here, the electrochemical performance and electronic structure information of MnHCF were studied in aqueous Zn-ion batteries (ZIBs). Based on the cyclic voltammetry and galvanostatic charge/discharge results, an activation of Fe-sites during beginning cycles was observed, and the capacity contribution of Fe-sites increases from 30% to 86% at C/20 during the first 10 cycles. The local geometric and electronic structure information of MnHCF was investigated by X-ray absorption spectroscopy (XAS) in a set of ex-situ electrodes. From Fe K-edge spectra, it shows a consistent oxidation and reduced state in charged and discharged electrodes, and this indicates that there is no apparent change for the local Fe-sites environment. However, the XAS spectra of Mn K-edge show apparent change after 10 cycles. Compared to the rhombohedral phase of Zinc hexacyanoferrate (ZnHCF), a -Zn-CN-Fe- structural framework was detected in the cycled MnHCF samples, and this indicates that a part of Zn replaced Mn-sites, because of the dissolution of the Mn-sites. The gradual activation of Fe-sites at the beginning cycles can be attributed to the alleviation spatial resistance with the dissolution of Mn-sites, and the replacement of Zn for Mn explains the decreasing capacity during cycling.</p>

1 **Electrochemical performance of Manganese Hexacyanoferrate**
2
3
4 **cathode material in aqueous Zn-ion battery**

5
6
7
8
9 **Min Li^(a), Rosalinda Sciacca^(b), Mariam Maisuradze^(a), Giuliana Aquilanti^(c),**
10
11 **Jasper Plaisier^(c), Mario Berrettoni^(d), Marco Giorgetti * ^(a)**

12
13
14
15
16
17 ^(a)Department of Industrial Chemistry “Toso Montanari”, University of Bologna, Viale
18
19
20 del Risorgimento 4, 40136 Bologna, Italy

21
22 ^(b) Department of Industrial Chemistry “Toso Montanari”, University of Bologna,
23
24
25 UOS Campus Di Rimini, via dei Mille 39, 47921 Rimini, Italy

26
27
28 ^(c)Elettra - Sincrotrone Trieste, s.s. 14, km 163.5, Basovizza 34149, Trieste, Italy

29
30
31 ^(d)School of Science and Technology, Chemistry Division, University of Camerino,
32
33
34 Camerino, Italy

35
36
37
38
39
40
41
42 *Corresponding author. Email: marco.giorgetti@unibo.it, phone +39 051 3093 666

43
44
45
46
47 **Keywords:** Sodium manganese hexacyanoferrate; Aqueous Zn-ion battery;
48
49
50 Mn/Fe-site study; ex-situ XAS spectra

1
2
3 **Abstract**
4
5
6

7 Manganese hexacyanoferrate (MnHCF) has attracted much attention as promising
8
9 cathode material for Li and Na ion batteries, owing to its low cost, environmental
10
11
12 friendliness, high specific capacity and voltage plateau. Here, the electrochemical
13
14
15 performance and electronic structure information of MnHCF were studied in aqueous
16
17
18 Zn-ion batteries (ZIBs). Based on the cyclic voltammetry and galvanostatic
19
20
21 charge/discharge results, an activation of Fe-sites during beginning cycles was
22
23
24 observed, and the capacity contribution of Fe-sites increases from 30% to 86% at
25
26
27 C/20 during the first 10 cycles. The local geometric and electronic structure
28
29
30 information of MnHCF was investigated by X-ray absorption spectroscopy (XAS) in
31
32
33 a set of ex-situ electrodes. From Fe K-edge spectra, it shows a consistent oxidation
34
35
36 and reduced state in charged and discharged electrodes, and this indicates that there is
37
38
39 no apparent change for the local Fe-sites environment. However, the XAS spectra of
40
41
42 Mn K-edge show apparent change after 10 cycles. Compared to the rhombohedral
43
44
45 phase of Zinc hexacyanoferrate (ZnHCF), a -Zn-CN-Fe- structural framework was
46
47
48 detected in the cycled MnHCF samples, and this indicates that a part of Zn replaced
49
50
51 Mn-sites, because of the dissolution of the Mn-sites. The gradual activation of Fe-sites
52
53
54 at the beginning cycles can be attributed to the alleviation spatial resistance with the
55
56
57 dissolution of Mn-sites, and the replacement of Zn for Mn explains the decreasing
58
59
60 capacity during cycling.
61
62
63
64
65

1. Introduction

Aqueous rechargeable metal-ion batteries (ARMBs) have giant potential in large-scale energy storage due to the advantages of low cost, safety, environmental benign and high ionic conductivity. To date, a variety of ARMBs based on many metal ions including naturally-abundant alkali metal ions (Na^+ and K^+)[1–4] and multivalent charge carriers (Zn^{2+} , Mg^{2+} , Al^{3+} , etc.) have been investigated [5–9]. Among different ARMBs, aqueous Zinc-ion batteries (ZIBs) are considered as some of the most promising candidates for stationary application, because of the unique properties of metallic zinc, which is an ideal anode material with high theoretical gravimetric and volumetric capacity of 820 mAh g^{-1} and 5855 mAh cm^{-3} , low electrochemical potential (-0.76 V vs. SHE), high abundance and intrinsic safety [10,11]. Meanwhile, the stripping-plating of Zn metal anode also shows good reversibility in mildly acidic aqueous solutions[12].

Among different cathode materials, Prussian blue analogues (PBAs) as bimetallic cyanides are considered as promising cathode material for Zn-ion batteries, due to their large ionic channels and interstices in the lattice, abundant redox-active sites, and strong structural stability[13,14] Copper hexacyanoferrate (CuHCF) and Zinc hexacyanoferrate (ZnHCF) were first investigated as cathode material in aqueous ZIBs by Wang et al.[15] and Liu et al.[16], and they found that unlike

1 manganese-based and vanadium-based materials, [6,17–19] CuHCF and ZnHCF
2
3 exhibited high operation voltage, which can reach 1.7 V. Manganese hexacyanoferrate
4
5 (MnHCF)[20–22], Cobalt hexacyanoferrate (CoHCF)[23] and Vanadium
6
7 hexacyanoferrate (VHCF)[24] have also been used as cathode materials for aqueous
8
9 ZIBs, and they do not only show a high discharge potential (>1.5 V), but also a
10
11 large-capacity due to the multi-redox active sites. However, most of PBAs are facing
12
13 the problem of capacity fading and short cycle lifespan during the Zn-ions insertion
14
15 and extraction in aqueous electrolyte. La Mantia and coworkers[25–27] have reported
16
17 a series of works about the structural and phase change of CuHCF during Zinc-ion
18
19 insertion. They found a new secondary phase was formed during insertion/extraction
20
21 of Zn^{2+} based on XRD data, but which are not well matched with the already reported
22
23 orthorhombic or monoclinic ZnHCF phases, and they proposed that the structural
24
25 changes can be related to the insertion of zinc-ions into the interstitial site and/or
26
27 replacement of Cu sites due to the dissolution of Cu^{2+} . Renman and coworkers[28]
28
29 studied the crystal structure changes of CuHCF by using operando synchrotron X-ray
30
31 diffraction (XRD. They found that the Zn^{2+} occupy both Fe $(\text{CN})_6$ vacancy site (4a)
32
33 and the cavity (8c), and during the discharge process, the change of occupancy for the
34
35 4a site (increasing) and the 8c site (decreasing) is quite opposite. They proposed that
36
37 the structural changes are associated with swapping of Zn^{2+} between the tunnels and
38
39 the vacant Fe $(\text{CN})_6$ sites. Thus, understanding the crystal distortion and phase
40
41 transformation of the electrode material can well explain the capacity fading problems
42
43 during cycling. However, determining exactly where Zn^{2+} resides within the
44
45
46
47
48
49
50
51
52
53
54
55
56
57
58
59
60
61
62
63
64
65

1 cavities/channels is not a straightforward task.
2
3
4
5

6 In this paper, the synthesis of MnHCF is described, as well as its application as
7
8 cathode material for ZIBs, in comparison with the other PBAs. MnHCF is composed
9
10 of only highly abundant metals and displays large capacity and high discharge
11
12 potential[29]. X-ray absorption spectroscopy (XAS) was used to study the
13
14 electrochemical-structural and electronic properties of MnHCF in aqueous ZIBs. As
15
16 XAS is a powerful tool that can be tuned to a chosen element, the physiochemical
17
18 properties and the local geometric and /or electronic structure of the selected element
19
20 can be obtained. Here, ex-situ XAS was used to record Mn, Fe and Zn k-edge spectra
21
22 at different charge and discharge states. By tracing the electron structural changes, we
23
24 can get information about local metal structural modifications during Zn^{2+} insertion
25
26 and release.
27
28
29
30
31
32
33
34
35
36

37 **2. Experimental**

38 **2.1 Synthesis of MnHCF and ZnHCF**

39
40
41 The synthesis of MnHCF was based on a simple and reproducible co-precipitation
42
43 method, as reported in ref [29]. 100 ml 0.1 M manganese sulfate monohydrate
44
45 ($MnSO_4 \cdot H_2O$) solution and 100 ml 0.1 M sodium ferrocyanide decahydrate
46
47 ($Na_4Fe(CN)_6 \cdot 10H_2O$) simultaneously added dropwise to an aqueous solution of
48
49 sodium sulfate (Na_2SO_4 , 0.1 M 100 mL) by using a peristaltic pump at a rate of 4 mL
50
51 min^{-1} . Both reagents and reaction batch were kept under N_2 atmosphere at constant
52
53
54
55
56
57
58
59
60
61
62
63
64
65

1 temperature (40 ± 2 °C) using a water bath. The obtained solution was aged for 5 days,
2
3 assuring complete decantation. Then the precipitate was collected via centrifugation at
4
5
6 4000 rpm and washed three times with distilled water, dried at 60 °C for 48 h.
7

8
9 ZnHCF was also synthesized by a co-precipitation method: 25 mM ZnCl₂ solution
10
11 added dropwise to a 25 mM K₃Fe(CN)₆ solution with stirring. A yellowish colloidal
12
13 solution was obtained and it was left standing overnight. The precipitated sample was
14
15 washed with deionized water and centrifuged several times in order to remove the
16
17 unreacted salts and separate the solid products. The precipitate was dried at 80 °C
18
19
20
21
22 overnight.
23

24 25 2.2 Electrode preparation and electrochemical tests 26

27
28 The electrochemical properties of the obtained material were evaluated in
29
30 three-electrode mode: the active material as working electrode, zinc sheet as reference
31
32 electrode and counter electrode. The working electrode was prepared by mixing the
33
34 active material (70%), super C65 (25%) and PTFE (5%) and grinding until we got
35
36 homogenous thin solid slice. Then we used a puncher to get 8 mm (diameter) pellets
37
38 with a mass density of around 5~10 mg/cm², then an aluminum mesh was used to fix
39
40 the pellet. Full coin cells were assembled by using metal Zn sheet as anode and
41
42 MnHCF and ZnHCF pellet as cathode in 3M ZnSO₄ electrolyte.
43
44
45
46
47
48

49
50 Cyclic voltammetry (CV) was performed by means of CHI Instruments Model 660.
51

52
53 The CV test was conducted in potential range 1~2.2 V (three-electrode) and 1-2 V
54
55 (coin cell) vs Zn²⁺/Zn in 3 M ZnSO₄ aqueous solution.
56
57

58
59 Galvanostatic cycling with potential limit (GCPL) was conducted in $1 < E < 1.9$ V vs
60
61
62
63
64
65

1 Zn²⁺/Zn potential window at different current densities. Cycling started after a rest
2
3 time (3 h) at OCP condition with a positive imposed current.
4
5

6 2.3 Characterization 7

8
9 A Microwave plasma-atomic emission spectrometer (MP-AES) 4210 was used to
10 detect the composition of the active material. During the test, three different
11 wavelengths were chosen for each element.
12
13
14
15

16 Infrared (IR) spectrum was measured using a Bruker Alpha FT-IR spectrometer in
17 ATR (Attenuated Total Reflectance) mode at a spectral range of 4000-400 cm⁻¹.
18
19

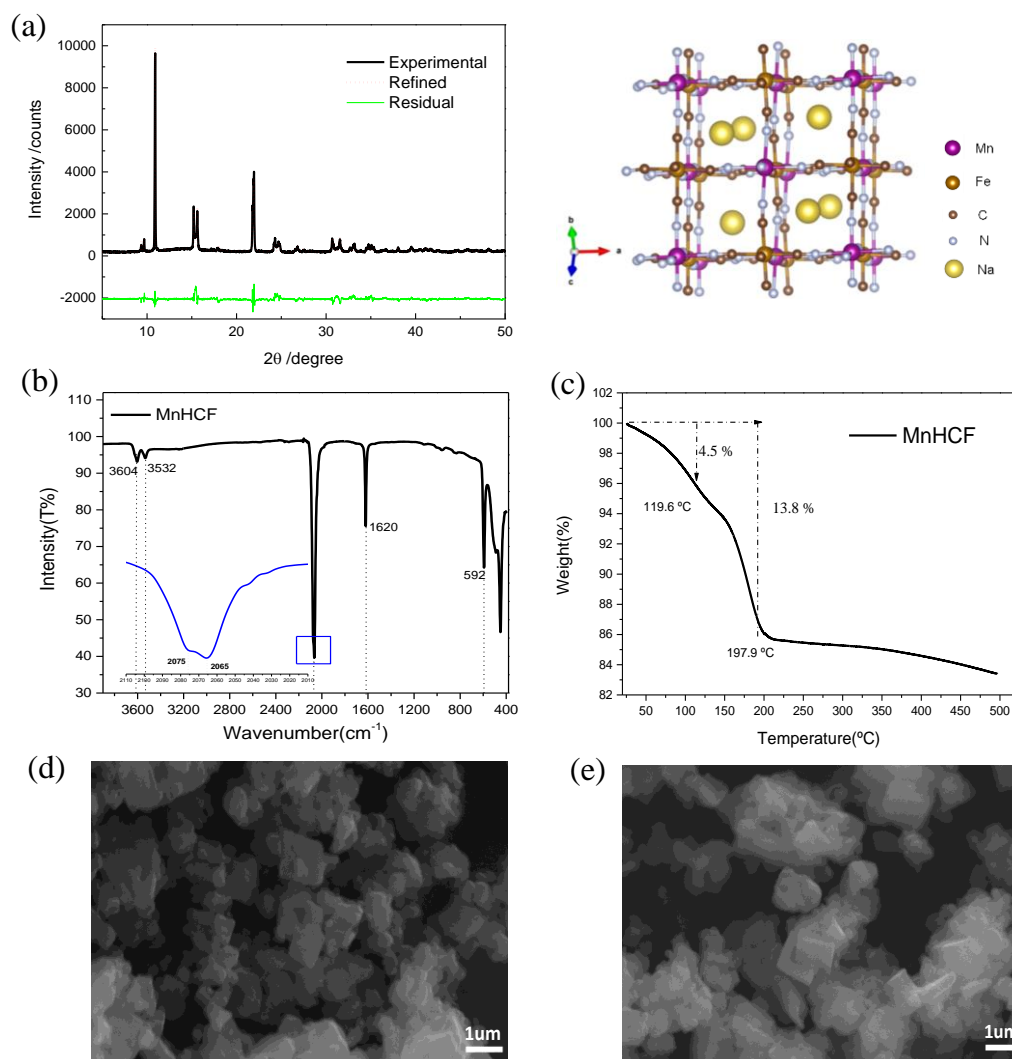
20 Thermogravimetric analysis (TGA) was performed in air atmosphere from room
21 temperature to 500 °C, with a heating rate of 5 °C min⁻¹, and rapid cooling.
22
23
24
25

26 Powder X-ray diffraction (PXRD) data were recorded by using a monochromatic
27 X-ray beam (wavelength of 1 Å) at the MCX beamline in ELETTRA synchrotron
28 Trieste (Italy)[30]. Data were collected in a capillary geometry, setting the spinner at
29 180 rpm. The X-ray diffraction pattern was collected consecutively in the range
30 5°<2θ<70°, with steps of 0.01° and an acquisition time of 1 s/step. The crystal
31 structure was refined using Fullprof Suite[31].
32
33
34
35
36
37
38
39
40
41
42
43

44 X-ray absorption spectroscopy (XAS) experiments were conducted at Elettra
45 Synchrotron Trieste (Italy), at XAFS beamline[32]. The storage ring was operated at
46 2.0 GeV in top-up mode with a typical current of 300 mA. Data were recorded at the
47 Fe, Mn and Zn K-edge in transmission mode using ionization chambers filled with a
48 mixture of Ar, N₂, and He to have 10, 70, and 95% of absorption in the I₀, I₁ and I₂
49 chambers, respectively. An internal reference of iron, manganese and zinc foil was
50
51
52
53
54
55
56
57
58
59
60
61
62
63
64
65

1 used for energy calibration in each scan. This allowed a continuous monitoring of the
2 energy during consecutive scans. The white beam was monochromatized using a fixed
3 exit monochromator equipped with a pair of Si (111) crystals. Spectra were collected
4 with a constant k-step of 0.3 nm^{-1} with 3 s per point acquisition time from 6345 to
5 7100 eV, from 6920 to 8350 eV, and from 9467 to 10897 eV around Mn, Fe and Zn
6 K-edges, respectively. XAS spectra were calibrated using the Athena program [33].
7
8
9
10
11
12
13
14
15
16
17
18
19
20
21
22

23 3. Result and Discussion



24
25
26
27
28
29
30
31
32
33
34
35
36
37
38
39
40
41
42
43
44
45
46
47
48
49
50
51
52
53
54
55
56
57
58
59 Figure 1. (a) XRPD pattern and Rietveld refinement on MnHCF powder with
60
61
62
63
64
65

1 tridimensional ball and stick structure (right); (b) IR spectrum of MnHCF; (c) TGA
2
3 curve of MnHCF; (d, e) SEM image of the as-prepared MnHCF.
4
5
6
7

8
9 The X-ray powder diffraction (XRPD) pattern of MnHCF is shown in figure 1(a).
10
11 Rietveld refinement was carried out to refine the lattice parameters and atomic
12 positions and the result showed that MnHCF has a monoclinic lattice (space group:
13
14 $P2_1/n$) with a, b, c and β equal to 10.571(6) Å, 7.463 (9) Å, 7.406 (9) Å and 92.10(8) °,
15
16 respectively. IR spectroscopy of MnHCF is shown in figure 1(b). Two small sharp
17
18 peaks occur around 3604 and 3532 cm^{-1} , which can be attributed to -O-H stretching
19
20 mode arising from surface water (non/weak-hydrogen bonded) and interstitial water.
21
22 Meanwhile, the peak at 1620 cm^{-1} is related to the bending mode of the -O-H group of
23
24 interstitial water. A distinguishable peak appears at around 2065 cm^{-1} ~ 2075 cm^{-1} ,
25
26 which is the characteristic peak of the $-\text{C}\equiv\text{N}$ group. Because the cyanide bridge is
27
28 extremely sensitive to its environment and oxidation states, the wavenumber of $-\text{C}\equiv\text{N}$
29
30 group here should represent the $\text{Mn}^{\text{II}}-\text{C}\equiv\text{N}-\text{Fe}^{\text{II}}$ group[34,35]. Thermogravimetric
31
32 analysis (TGA) of the prepared sample shows two distinct weight-loss events at
33
34 around 120 °C and 200 °C (figure 1(c)), which are ascribed to the loss of absorbed
35
36 water and interstitial/structural water, respectively, around 13.8% of the total weight.
37
38 Combining this with the composition results obtained from ICP-OES measurement
39
40 (table S1), the chemical formulation of MnHCF is $\text{Na}_{1.47} \text{Mn} [\text{Fe} (\text{CN})_6]_{0.88} \cdot 2.6\text{H}_2\text{O}$.
41
42 The morphology of the material was studied by scanning electron microscope (SEM),
43
44 as shown in figure 1(d, e). It can be seen that some cubic-shaped particles are
45
46
47
48
49
50
51
52
53
54
55
56
57
58
59
60
61
62
63
64
65

distributed in the range of 100-1000 nm.

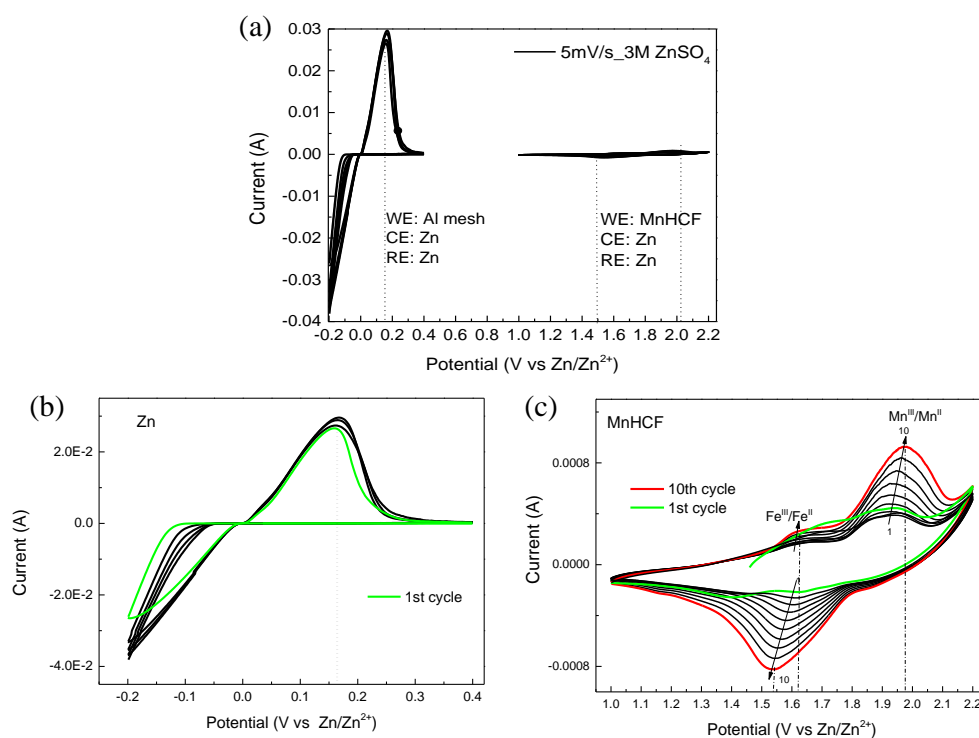


Figure 2. (a) CV curves of MnHCF and Zn plating/stripping at scan rate of 5 mV s⁻¹ in 3M ZnSO₄ electrolyte; (b) zoom-in CV curve of Zn plating/stripping; (c) zoom-in CV curve of MnHCF.

Electrochemical reversibility and stability of as-prepared MnHCF and metal Zn anode were first investigated in a three-electrode system in 3 M ZnSO₄ aqueous electrolyte, in which Zn sheet was used as both counter and reference electrode, as shown in figure 2(a). In the case of Zn anode (figure 2(b)), there is one apparent oxidation peak around 0.16 V (vs. Zn²⁺/Zn), which is attributed to the dissolution of zinc (stripping). The intensity of the reduction peak of Zn²⁺ keeps increasing along with the negative shift in the potential below 0 V (vs. Zn²⁺/Zn), which is ascribed to the deposition of

zinc on the electrode (plating). Here, Zinc metal anode shows good stripping-plating reversibility in 3M ZnSO₄ electrolyte. CV curves of MnHCF are shown in figure 2(c), two oxidation peaks are observed at around 1.62 V and 1.95 V, and one wide reduction peak is at around 1.6 V, which can attributed to the redox couple of the low-spin Fe²⁺/Fe³⁺ and high-spin Mn²⁺/Mn³⁺, respectively[20,36]. Current intensity of cathode redox peaks is increasing with cycles going, and it is probably due to the gradual activation of the electrode. The same phenomenon was also reported for MnO₂ and ZnMn₂O₄ [37,38].

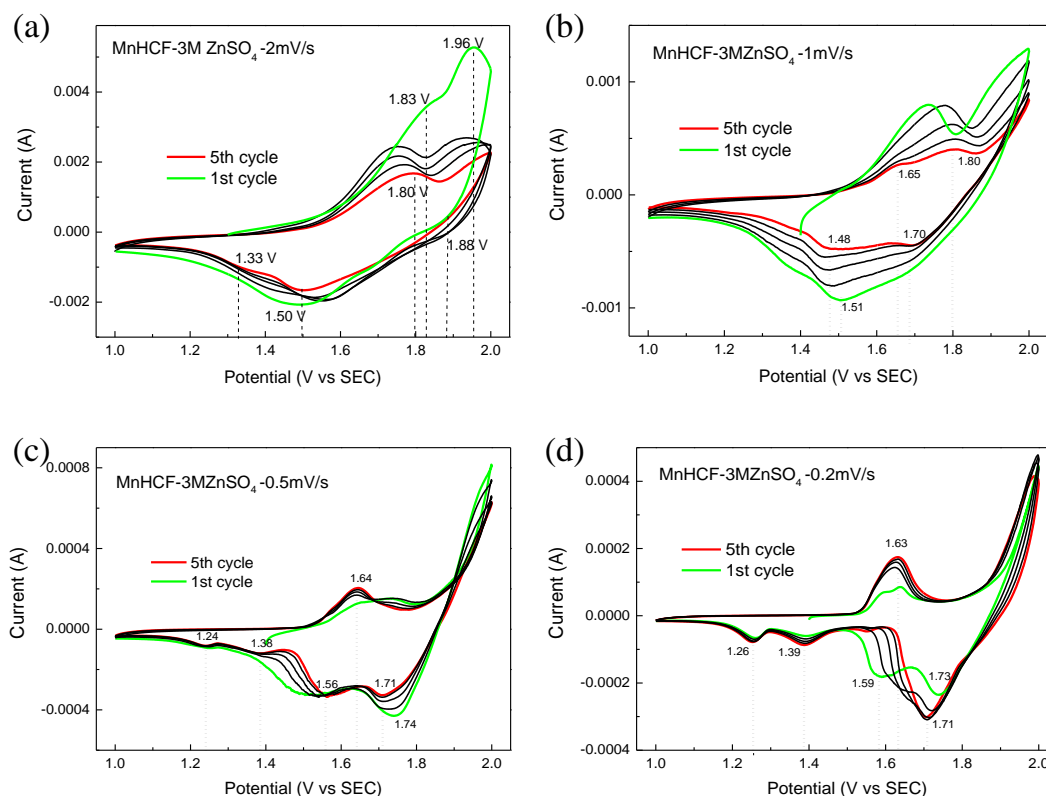
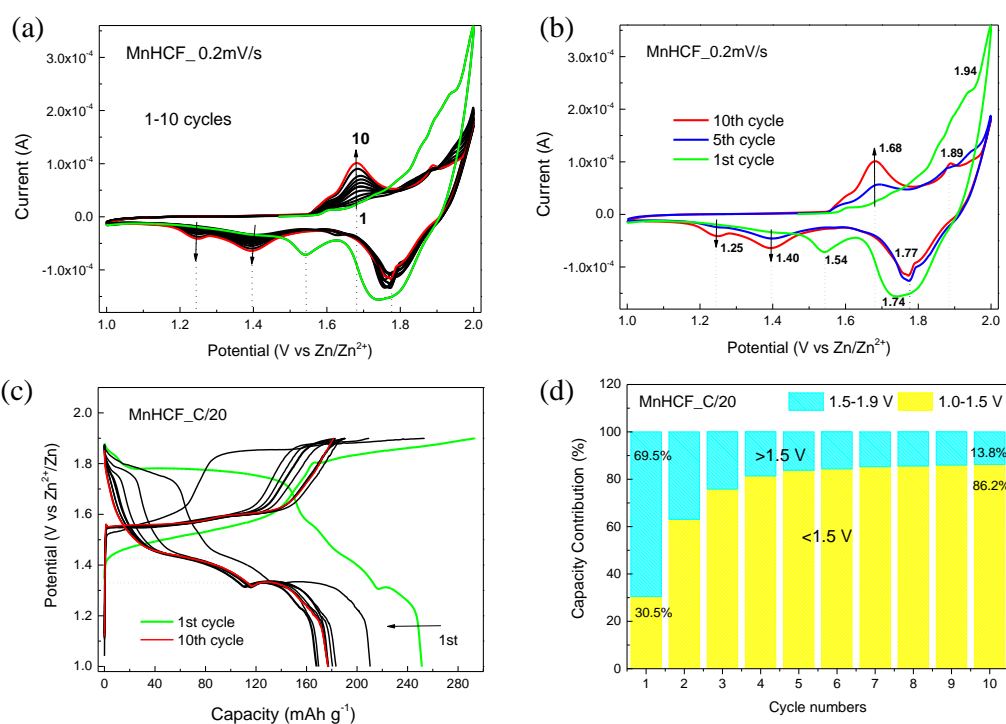


Figure 3. CV curves of MnHCF full-cell at different scan rate: (a) 2 mV s⁻¹, (b) 1 mV s⁻¹, (c) 0.5 mV s⁻¹ and (d) 0.2 mV s⁻¹.

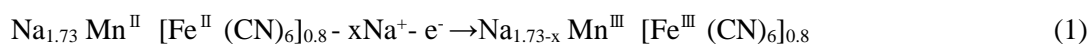
Full-cells were assembled by using metal Zn sheet as anode and MnHCF as cathode

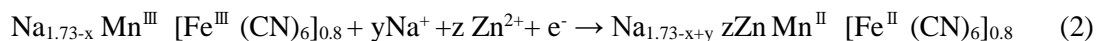
1 in 3M ZnSO₄ electrolyte. CV profiles were obtained at different scan rates from 2 to
 2
 3
 4 0.2 mV/s. With decreasing scan rate, a gradual change of redox peaks was observed,
 5
 6 both in current intensity and peak position. As shown in figure 3(a), two pairs of
 7
 8 redox peaks were observed at 1.83/1.50 V and 1.96/1.88 V at the first cycle of 2 mV/s,
 9
 10 that becomes progressively one wide anode peak at 1.80 V and two cathode peaks at
 11
 12 1.33 V and 1.50 V, as observed at the 5th cycle. When the scan rate decreases to 1
 13
 14 mV/s, two pair of redox peaks were observed at 1.65/1.48 V and 1.80/1.70 V at 5th
 15
 16 cycle. As the scan rate reduces to 0.5 mV/s and 0.2 mV/s, only one anode peak
 17
 18 appeared at around 1.63V, but two new cathode peaks were observed at 1.26 V and
 19
 20 1.39 V, and the peak at around 1.56 V gradually disappeared. Similar to the
 21
 22 three-electrode system, current intensity of redox peaks was increasing with the
 23
 24 number of cycles at 0.2mV/s.
 25
 26
 27
 28
 29
 30
 31
 32
 33
 34
 35



1 Figure 4. (a) CV curves of MnHCF full-cell at 0.2 mVs⁻¹ for 10 cycles; (b) 1st, 5th and
2
3 10th cycle CV curves at 0.2 mVs⁻¹; (c) first 10 cycles of Galvanostatic
4
5 charge/discharge curves of MnHCF at C/20; (d) the corresponding discharge capacity
6
7 contribution of different voltage range at C/20.
8
9

10
11
12
13
14 In order to trace the change of CV curves at the same current density, a new MnHCF
15
16 full cell was tested at a scan rate of 0.2 mV/s for 10 cycles. As shown in figure 4 (a, b),
17
18 the CV profile in the first cycle is slightly different from the following ones. The
19
20 the CV profile in the first cycle is slightly different from the following ones. The
21
22 oxidation peak at 1.94 V can be related to the extraction of Na⁺ from electrode during
23
24 the first charge process (Equation 1), while the two reduction peaks at 1.74 V and 1.54
25
26 V during the first discharge process can be attributed to the insertion of Zn²⁺ and Na⁺
27
28 (Equation 2), respectively. Two oxidation peaks at 1.68 V and 1.89 V were observed
29
30 in the successive cycles, which might correspond to Zn-extraction from MnHCF
31
32 cathode as the Fe^{II} and Mn^{II} states undergo oxidation to the Fe^{III} and Mn^{III} states.
33
34 Furthermore, except for the reduction peak at 1.77 V, two new reduction peaks at 1.40
35
36 V and 1.25 V appeared, and in light of the literature reports [21,39], they can be
37
38 attributed to the reduction of Fe³⁺ to Fe²⁺. The current intensity of these two peaks
39
40 was increasing cycle by cycle, as well as the oxidation peak at 1.68 V. This behavior
41
42 was maybe related to the gradual activation of the electrode and/or the structural
43
44 transition with insertion/extraction of Zn-ions.
45
46
47
48
49
50
51
52
53
54
55
56
57





The Zn/MnHCF cell was fabricated under open-air conditions, and displayed an open-circuit potential (OCP) around 1.30 V. Figure 4 (c) shows the first 10 charge/discharge profiles of MnHCF in the potential range of 1.0-1.9 V vs. Zn^{2+}/Zn at C/20 rate. The first two charges and discharges of MnHCF showed capacity above 200 mAh/g, and this maybe because of the partial decomposition of electrolyte and extraction/insertion of both Na^+ and Zn^{2+} at the same time. From the third cycle, the discharge capacity was centered at around 176 mAhg⁻¹, and the discharge plateaus were also changed with cycling. A discharge plateau at around 1.78 V was initially observed, and then it disappeared gradually. Meanwhile, two new discharge plateaus around 1.42 V and 1.33V have shown up, which are consistent with the CV peaks (figure 4a). Based on the reduction peaks potential, we calculated the capacity contribution at different voltage range, as shown in figure 4(d). The total discharge capacity during the whole cycling process is divided into two main contributions: 1.0-1.5 V and 1.5-1.9 V, which are attributed to the $\text{Fe}^{2+/3+}$ and $\text{Mn}^{2+/3+}$ redox couples, respectively. The capacity contribution of $\text{Fe}^{2+/3+}$ increases from 30% at the beginning to 86% at 10th cycle, which is consistent with the CV data where current intensity of $\text{Fe}^{2+/3+}$ increases with cycles. Thus, we postulate that there is an activation of Fe-sites within MnHCF structure during Zn-ions insertion/extraction. Meanwhile, the Mn-sites experience a deactivating process and which is probably due to the dissolution of Mn-sites or the change of local environment of Mn-sites, which are discussed later.

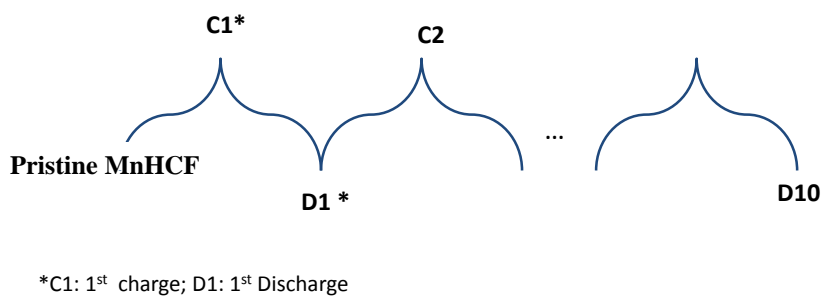


Figure 5. Schematic diagram of samples of different charge/discharge states.

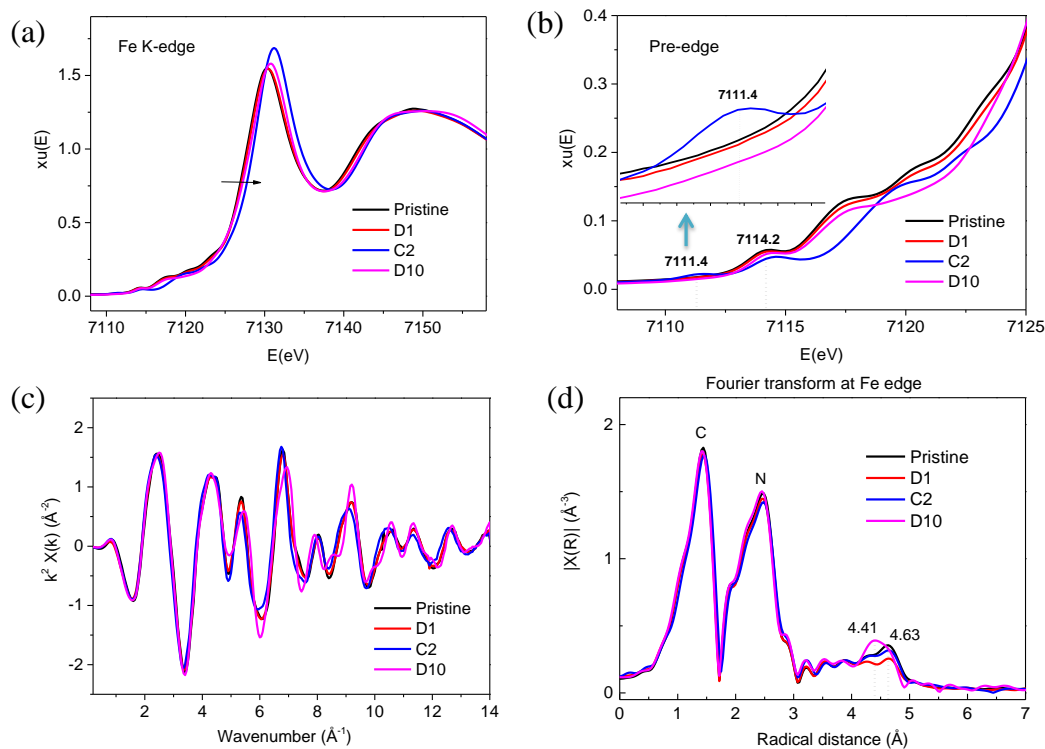


Figure 6. (a) Ex-situ XANES of MnHCF powder and formulated electrodes at the Fe K-edge; (b) Zoom in the pre-edge feature of Fe K-edge; (c) k^2 -weighted EXAFS signals and (d) corresponding Fourier transforms (FTs).

The electrochemical performance of an electrode material is derived from the combination of structures, electronic properties and the reversible evolution of

1 active-sites upon the charge and discharge process. In order to detect the change of the
2
3 structure and the electronic properties of the active-sites inside MnHCF during
4
5 cycling, ex-situ XAS spectra were recorded at the Fe, Mn and Zn K-edge at different
6
7 charge and discharge states, as represented by the scheme in Fig. 5. Fe K-edge spectra
8
9 were recorded at D1, C2 and D10 states, and the pre-edge and k^2 -weighted EXAFS
10
11 signal as well as the corresponding FTs are shown in figure 6 (b-d). As expected, in
12
13 figure 6(a) the C2 sample shows an oxidized state of Fe with respect to pristine and
14
15 discharged ones; the other discharged samples displayed similar spectra as the pristine
16
17 sample, indicating that there were no obvious changes of Fe local environment during
18
19 the insertion/extraction of Zn-ions. The pre-edge peaks of Fe at 7111.4 eV and 7114.2
20
21 eV are attributed to the $1s \rightarrow e_g$ and $1s \rightarrow t_{2g}$ electronic transitions of low-spin state Fe^{III} ,
22
23 and only C2 shows the 7111.4 eV peak as shown in figure 6(b). The FTs at Fe
24
25 K-edges are shown in figure 6(d), based on the framework structure of MnHCF
26
27 (-Fe-C-N-Mn-), the first two peaks are attributed to the carbon first shell (Fe-C) and
28
29 nitrogen (Fe-C-N), while the third peak is related to manganese (Fe-C-N-Mn) [29].
30
31 The D10 sample shows a little different shape of the third peak with respect to other
32
33 cycled samples, which might reflect the Mn-Zn replacement during the
34
35 insertion/extraction of Zn-ions.
36
37
38
39
40
41
42
43
44
45
46
47
48
49
50
51
52
53
54
55
56
57
58
59
60
61
62
63
64
65

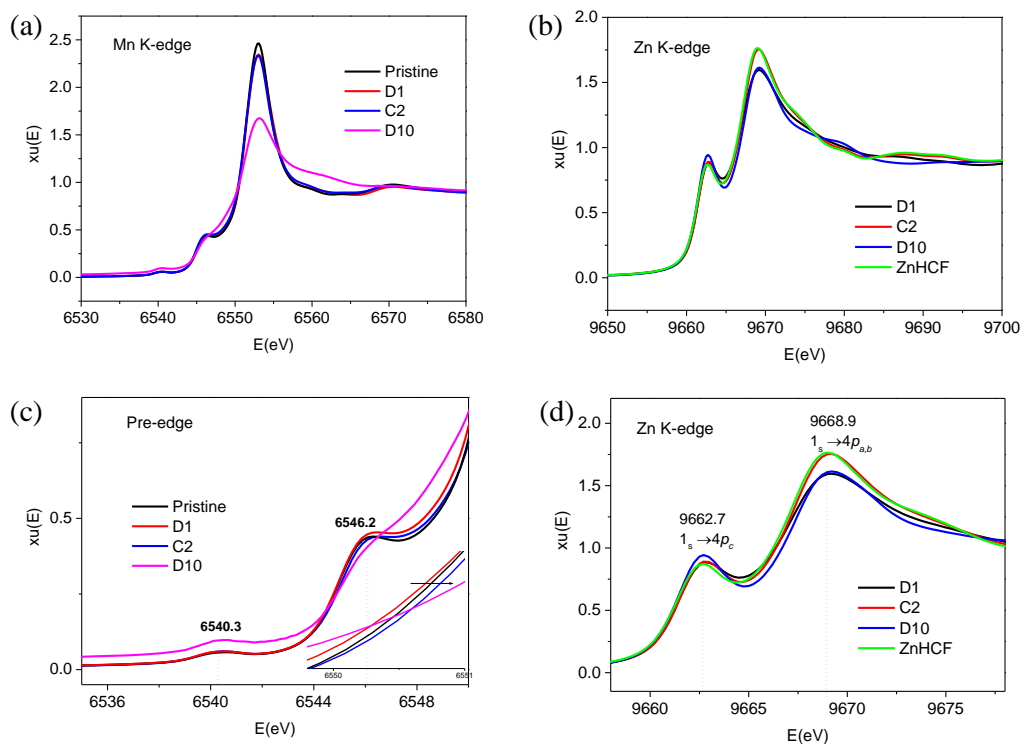


Figure 7. (a) (b) Ex-situ XANES of MnHCF powder and formulated electrodes at the Mn and Zn K-edge; (c) pre-edge feature of Mn K-edge; (d) Zoom in the Zn K-edge.

Mn and Zn XANES K-edge spectra were recorded at same charge/discharge states (D1, C2 and D10) and are displayed in Fig. 7 (a,b) and (c,d), respectively. As well known, the rising edge portion of the XANES has a strong contribution from the $1s$ to $4p$ transition, and factors that affect the shape and energy of selected features: oxidation state, coordination number and geometry, and covalency[40]. The pre-edge peaks (Figure 7c) at 6540.3 eV and 6546.2 eV are considered to be the transition into T_{2g}/e_g and $4p$ orbitals in Mn^{2+} species, respectively. Overall, the spectra are nearly identical in both series of measurements. The only exception regards the D10 sample at the Mn K-edge, which displays a different curve shape. Therefore it is suggested that the local structure of manganese in pristine, D1, and C2 samples is similar and so

1 does the local charge associated to the metal, because no obvious energy shift was
2
3 observed. The different curve shape in D10 might be attributed to the change of local
4
5 coordination and geometry with insertion/extraction of Zn-ions.
6
7

8
9
10
11 We got the edge step values of Fe/Mn/Zn K-edge at different charge and discharge
12
13 states, and these values are proportional to the content of metal-sites inside the
14
15 electrode material. As it is shown in table S2, the value for Fe K-edge shows almost
16
17 no changes at D1, C2 and D10 states. However, the edge step value for Mn K-edge
18
19 was reduced from pristine 0.215 to 0.00793 (D10), and this indicates that the Mn
20
21 content inside the electrode was significantly decreased due to the dissolution. This
22
23 was confirmed from the post-mortem analysis of electrolyte (table S3) in which Mn
24
25 was detected inside the electrolyte after cycling. Thus, the low intensity of Mn K-edge
26
27 at D10 state is related to the low Mn content inside the electrode.
28
29
30
31
32
33
34
35
36
37
38

39 The hypothesis of the Mn to Zn replacement is confirmed by looking at the XANES
40
41 spectra at the Zn K-edge, showed in figure 7 (b) (d). XANES spectra measure the
42
43 transitions of electron from Zn 1s to unoccupied 4p states, because the 3d orbitals are
44
45 completely filled[41,42]. In order to have a reference to detect the local environment
46
47 of Zn inside MnHCF structure, we synthesized the rhombohedral zinc
48
49 hexacyanoferrate (ZnHCF). Surprisingly, all the samples show the same XANES
50
51 spectra as ZnHCF, even the D1 and C2 samples, which indicates that even at the
52
53 beginning of cycling, there is a formation of the ZnHCF phase inside the MnHCF
54
55
56
57
58
59
60
61
62
63
64
65

1 structure. Where does the manganese go during the cycling? Elemental analysis
2
3 conducted on the electrolyte solution bath as well as by using the edge step values of
4
5 the measurements at both Mn and Zn K-edge (table S2), confirm dissolution of the
6
7 Mn with concomitant enrichment of the Zn during cycling. A similar result was also
8
9 reported by Shu et al.[22] from ex-situ XPS spectra: Zn was not extracted completely
10
11 at charged state, some residues exist in the MnHCF framework, and there is even a
12
13 part of the Zn substituting the Mn-sites. Based on the edge step we got for the Zn
14
15 K-edge at different charge/discharge states, there was residual Zn at the C2 state, and
16
17 the value was increased from D1 to D10 (table S2). The Corresponding FT's of
18
19 k^2 -weighted EXAFS signal of Mn K-edge and Zn K-edge (figure S1) show the same
20
21 peak position for all the samples and the three peaks can be attributing to the nitrogen
22
23 (Mn-N), carbon (Mn-N-C) and iron (Mn-N-C-Fe). Overall, from the XAS
24
25 investigations, we can conclude that there is a part of Zn substitutiug Mn, forming the
26
27 Zn-N-C-Fe structural framework, which is characteristic of the rhombohedral ZnHCF
28
29
30
31
32
33
34
35
36
37
38
39 phase.
40
41
42
43
44
45
46
47
48
49
50
51
52
53
54
55
56
57
58
59
60
61
62
63
64
65

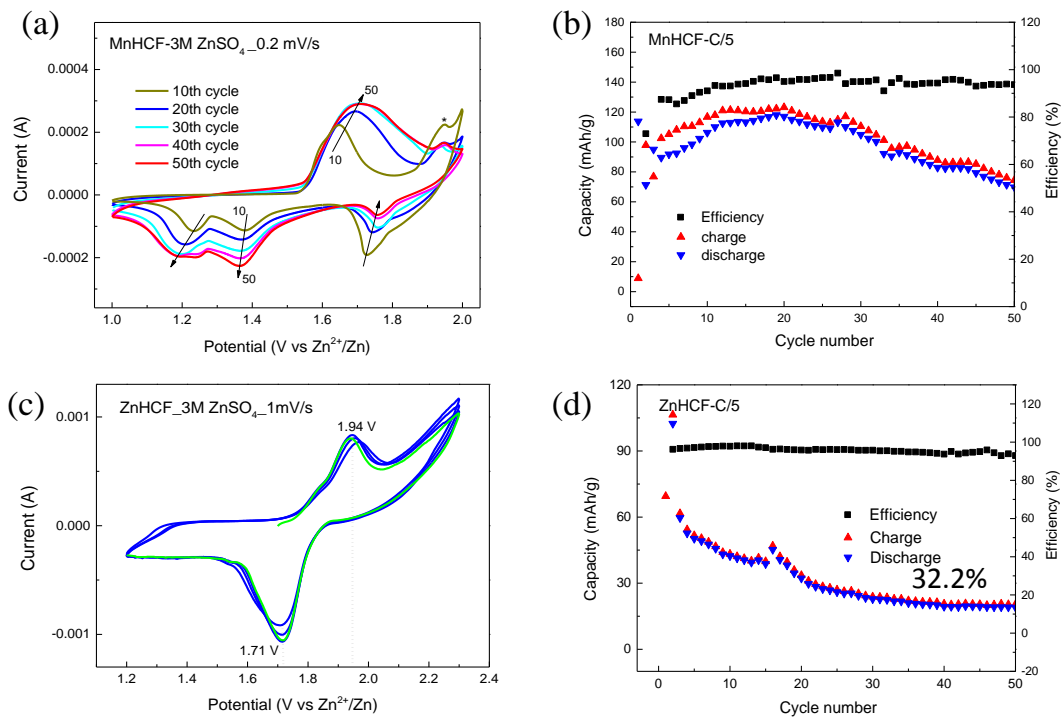


Figure 8. (a) CV curves of MnHCF full-cell at 0.2 mV s⁻¹ from 10th to 50th cycles; (b) cycling performance of MnHCF at C/5; (c) CV curve of ZnHCF at 1 mV/s; (d) cycling performance of ZnHCF at C/5 rate;.

The stability of MnHCF fuel-cell was tested through both CV and galvanostatic charge/discharge, as shown in figure 8(a, b). The redox peaks from the 10th to the 50th cycle show a similar trend as the first 10 cycles,. The current intensity of the anode peak at around 1.7 V and two reduction peaks at 1.20-1.40 V are increasing within the first 30 cycles, and after that the current intensity reaches a stable state. Meanwhile, the reduction peak at 1.70-1.75 V keeps decreasing, and becomes stable after 30 cycles. Based on the report [43], the gradual activation of Fe-sites at the early cycles, can be attributed to the alleviation of spatial resistance with the dissolution of Mn-sites. But, with substitution by Zn-ions, the activation process was confined. The

1 cycling performance of MnHCF at C/5 is shown in figure 8(b). The charge and
2
3 discharge curves show an increasing trend from the 3rd~20th cycle, and after 20cycles,
4
5 the curve starts to decrease gradually. The discharge capacity is increased from 110
6
7 mAhg⁻¹ at 10th cycle, to around 115 mAhg⁻¹ at 20th cycle, and then decreased to 70
8
9 mAhg⁻¹ at 50th cycle. We found that the CV data is closely related to the galvanostatic
10
11 charge and discharge data, and the peak current increasing or decreasing is reflected
12
13 on the changing of capacity. Thus, from the data above, we can conclude that the
14
15 activation of Fe-sites mainly happened during the first 20 cycles at C/5, and the
16
17 decrease of the capacity can be related to the Zn-replacement of Mn-site inside the
18
19 structure.
20
21
22
23
24
25
26
27
28
29
30

31 To confirm the low capacity of Zn-substituted MnHCF, the electrochemical
32
33 performance of pure ZnHCF was investigated, as shown in figure 8(c, d). Contrary to
34
35 the monoclinic structure of MnHCF, ZnHCF shows a rhombohedral structure (space
36
37 group: R-3C) with a/b, c and γ equal to 12.5795(3) Å, 33.05134 (1) Å and 120°,
38
39 respectively (figure S2 (a)). The CV curves of ZnHCF are stable and only one pair of
40
41 redox peaks was observed at 1.94/1.71 V at 1 mV/s. The galvanostatic charge and
42
43 discharge of ZnHCF at C/5 is shown in figure S2(b), with a discharge capacity of
44
45 around 60 mAh g⁻¹, discharge plateau around 1.71 V. Cycling performance is shown
46
47 in figure 8(d). The capacity fading was considerably fast, and only around 33%
48
49 capacity was retained after 50cycles, due to the dissolution of ZnHCF, as suggested by
50
51 Zhang and Ni et al [16,44] and this also explains the capacity fading of MnHCF
52
53
54
55
56
57
58
59
60
61
62
63
64
65

1 during cycling, as shown in figure 8(a,b).
2
3
4
5

6 **4. Conclusion**

7
8
9 The Electrochemical performance and electronic structure information of MnHCF
10 were studied in aqueous Zn-ion batteries. From the cycling voltammetry and
11 galvanostatic charge/discharge data, we found the gradual activation of Fe-sites and
12 the deactivation of Mn-sites. The capacity contribution of Fe-sites increased from 30%
13 to 86% during the first 10 cycles at C/20. The cycling stability of MnHCF was tested
14 at C/5 for 50 cycles, and it shows an increasing capacity during the first 20 cycles,
15 around 70% of capacity was retained after 50cycles. The activation of Fe-sites at the
16 starting cycles can be attributed to the alleviation of spatial resistance, caused by the
17 dissolution of Mn-sites. Based on the XAS analysis, the local environment of Fe-site
18 didn't change a lot, while hte Mn K-edge spectra had obvious changes at D10 state,
19 and -Zn-NC-Fe- structure was detected in all the cycled samples. These results
20 confirmed that there is partial replacement of Mn by Zn during charge/discharge
21 process, and this also explained the decreasing of capacity of MnHCF during the
22 cycling.
23
24
25
26
27
28
29
30
31
32
33
34
35
36
37
38
39
40
41
42
43
44
45
46
47
48
49

50 **Acknowledgements.**

51
52 Measurements at ELETTRA were supported by in-house research. This research was
53 funded by the University of Bologna, RFO funding.
54
55
56
57
58
59
60
61
62
63
64
65

Appendix A. Supplementary data

Supplementary data related to this article can be found at

5. References

- [1] Rechargeable Lithium Batteries with Aqueous Electrolytes Author (s): Wu Li , J . R . Dahn and D . S . Wainwright Published by : American Association for the Advancement of Science Stable URL : <http://www.jstor.org/stable/2885126> JSTOR is a not-for-profi, 264 (2016) 1115–1118.
- [2] M.H. Lee, S.J. Kim, D. Chang, J. Kim, S. Moon, K. Oh, K.Y. Park, W.M. Seong, H. Park, G. Kwon, B. Lee, K. Kang, Toward a low-cost high-voltage sodium aqueous rechargeable battery, *Mater. Today*. 29 (2019) 26–36. <https://doi.org/10.1016/j.mattod.2019.02.004>.
- [3] L. Wang, Y. Lu, J. Liu, M. Xu, J. Cheng, D. Zhang, J.B. Goodenough, A superior low-cost cathode for a Na-Ion battery, *Angew. Chemie - Int. Ed.* 52 (2013) 1964–1967. <https://doi.org/10.1002/anie.201206854>.
- [4] A. Eftekhari, Potassium secondary cell based on Prussian blue cathode, *J. Power Sources*. 126 (2004) 221–228. <https://doi.org/10.1016/j.jpowsour.2003.08.007>.
- [5] Y. Mizuno, M. Okubo, E. Hosono, T. Kudo, K. Oh-Ishi, A. Okazawa, N. Kojima, R. Kurono, S.I. Nishimura, A. Yamada, Electrochemical Mg²⁺ intercalation into a bimetallic CuFe Prussian blue analog in aqueous electrolytes, *J. Mater. Chem. A*. 1 (2013) 13055–13059.

- 1 <https://doi.org/10.1039/c3ta13205f>.
- 2
- 3 [6] C. Xu, B. Li, H. Du, F. Kang, Energetic zinc ion chemistry: The rechargeable
- 4 zinc ion battery, *Angew. Chemie - Int. Ed.* 51 (2012) 933–935.
- 5
- 6 <https://doi.org/10.1002/anie.201106307>.
- 7
- 8
- 9 [7] N. Kuperman, P. Padigi, G. Goncher, D. Evans, J. Thiebes, R. Solanki, High
- 10 performance Prussian Blue cathode for nonaqueous Ca-ion intercalation battery,
- 11 *J. Power Sources.* 342 (2017) 414–418.
- 12
- 13 <https://doi.org/10.1016/j.jpowsour.2016.12.074>.
- 14
- 15 [8] W.J. Li, S.L. Chou, J.Z. Wang, Y.M. Kang, J.L. Wang, Y. Liu, Q.F. Gu, H.K.
- 16 Liu, S.X. Dou, Facile method to synthesize na-enriched $\text{Na}_{1+x}\text{FeFe}(\text{CN})_6$
- 17 frameworks as cathode with superior electrochemical performance for
- 18 sodium-ion batteries, *Chem. Mater.* 27 (2015) 1997–2003.
- 19
- 20 <https://doi.org/10.1021/cm504091z>.
- 21
- 22 [9] Y. Hu, D. Ye, B. Luo, H. Hu, X. Zhu, S. Wang, L. Li, S. Peng, L. Wang, A
- 23 Binder-Free and Free-Standing Cobalt Sulfide@Carbon Nanotube Cathode
- 24 Material for Aluminum-Ion Batteries, *Adv. Mater.* 30 (2018) 1–6.
- 25
- 26 <https://doi.org/10.1002/adma.201703824>.
- 27
- 28 [10] R. Trócoli, F. La Mantia, An aqueous zinc-ion battery based on copper
- 29 hexacyanoferrate, *ChemSusChem.* 8 (2015) 481–485.
- 30
- 31 <https://doi.org/10.1002/cssc.201403143>.
- 32
- 33 [11] B. Tang, L. Shan, S. Liang, J. Zhou, Issues and opportunities facing aqueous
- 34 zinc-ion batteries, *Energy Environ. Sci.* 12 (2019) 3288–3304.
- 35
- 36
- 37
- 38
- 39
- 40
- 41
- 42
- 43
- 44
- 45
- 46
- 47
- 48
- 49
- 50
- 51
- 52
- 53
- 54
- 55
- 56
- 57
- 58
- 59
- 60
- 61
- 62
- 63
- 64
- 65

1 <https://doi.org/10.1039/c9ee02526j>.

- 2
3 [12] J. Shin, J. Lee, Y. Park, J.W. Choi, Aqueous zinc ion batteries: Focus on zinc
4 metal anodes, *Chem. Sci.* 11 (2020) 2028–2044.
5
6 <https://doi.org/10.1039/d0sc00022a>.
- 7
8
9 [13] M. Giorgetti, L. Guadagnini, D. Tonelli, Structural characterization of
10 electrodeposited copper hexacyanoferrate films by using a spectroscopic
11 multi-technique approach w, (2012) 5527–5537.
12
13 <https://doi.org/10.1039/c2cp24109a>.
- 14
15 [14] M. Berrettoni, M. Giorgetti, S. Zamponi, P. Conti, D. Ranganathan, A. Zanotto,
16 M.L. Saladino, E. Caponetti, C. Fisica, V. Uni, Synthesis and Characterization
17 of Nanostructured Cobalt Hexacyanoferrate, (2010) 6401–6407.
18
19 [15] Z. Jia, B. Wang, Y. Wang, Copper hexacyanoferrate with a well-defined open
20 framework as a positive electrode for aqueous zinc ion batteries, *Mater. Chem.*
21 *Phys.* 149 (2015) 601–606.
22
23 <https://doi.org/10.1016/j.matchemphys.2014.11.014>.
- 24
25 [16] L. Zhang, L. Chen, X. Zhou, Z. Liu, Towards high-voltage aqueous metal-ion
26 batteries beyond 1.5 V: The zinc/zinc hexacyanoferrate system, *Adv. Energy*
27 *Mater.* 5 (2015) 1–5. <https://doi.org/10.1002/aenm.201400930>.
28
29 [17] C. Wei, C. Xu, B. Li, H. Du, F. Kang, Preparation and characterization of
30 manganese dioxides with nano-sized tunnel structures for zinc ion storage, *J.*
31 *Phys. Chem. Solids.* 73 (2012) 1487–1491.
32
33 <https://doi.org/10.1016/j.jpccs.2011.11.038>.
- 34
35
36
37
38
39
40
41
42
43
44
45
46
47
48
49
50
51
52
53
54
55
56
57
58
59
60
61
62
63
64
65

- 1 [18] F. Wan, L. Zhang, X. Dai, X. Wang, Z. Niu, J. Chen, Aqueous rechargeable
2
3 zinc/sodium vanadate batteries with enhanced performance from simultaneous
4
5 insertion of dual carriers, *Nat. Commun.* 9 (2018) 1–11.
6
7 <https://doi.org/10.1038/s41467-018-04060-8>.
8
9
- 10 [19] J. Zhou, L. Shan, Z. Wu, X. Guo, G. Fang, S. Liang, Investigation of V₂O₅ as
11
12 a low-cost rechargeable aqueous zinc ion battery cathode, *Chem. Commun.* 54
13
14 (2018) 4457–4460. <https://doi.org/10.1039/c8cc02250j>.
15
16
17
- 18 [20] Z. Hou, X. Zhang, X. Li, Y. Zhu, J. Liang, Y. Qian, Surfactant widens the
19
20 electrochemical window of an aqueous electrolyte for better rechargeable
21
22 aqueous sodium/zinc battery, *J. Mater. Chem. A.* 5 (2017) 730–738.
23
24
25 <https://doi.org/10.1039/c6ta08736a>.
26
27
- 28 [21] Q. Li, K. Ma, G. Yang, C. Wang, High-voltage non-aqueous
29
30 Zn/K_{1.6}Mn_{1.2}Fe(CN)₆ batteries with zero capacity loss in extremely long
31
32 working duration, *Energy Storage Mater.* 29 (2020) 246–253.
33
34
35 <https://doi.org/10.1016/j.ensm.2020.04.030>.
36
37
- 38 [22] W. Li, C. Xu, X. Zhang, M. Xia, Z. Yang, H. Yan, H. Yu, L. Zhang, W. Shu, J.
39
40 Shu, Sodium manganese hexacyanoferrate as Zn ion host toward aqueous
41
42 energy storage, *J. Electroanal. Chem.* 881 (2021).
43
44
45 <https://doi.org/10.1016/j.jelechem.2020.114968>.
46
47
- 48 [23] L. Ma, S. Chen, C. Long, X. Li, Y. Zhao, Z. Liu, Z. Huang, B. Dong, J.A.
49
50 Zapfen, C. Zhi, Achieving High-Voltage and High-Capacity Aqueous
51
52 Rechargeable Zinc Ion Battery by Incorporating Two-Species Redox Reaction,
53
54
55
56
57
58
59
60
61
62
63
64
65

- 1 Adv. Energy Mater. 9 (2019). <https://doi.org/10.1002/aenm.201902446>.
- 2
- 3 [24] Y. Zhang, Y. Wang, L. Lu, C. Sun, D.Y.W. Yu, Vanadium hexacyanoferrate
- 4
- 5
- 6 with two redox active sites as cathode material for aqueous Zn-ion batteries, J.
- 7
- 8
- 9 Power Sources. 484 (2021) 229263.
- 10
- 11 <https://doi.org/10.1016/j.jpowsour.2020.229263>.
- 12
- 13
- 14 [25] G. Kasiri, R. Trócoli, A. Bani Hashemi, F. La Mantia, An electrochemical
- 15
- 16
- 17 investigation of the aging of copper hexacyanoferrate during the operation in
- 18
- 19
- 20 zinc-ion batteries, *Electrochim. Acta.* 222 (2016) 74–83.
- 21
- 22 <https://doi.org/10.1016/j.electacta.2016.10.155>.
- 23
- 24
- 25 [26] R. Trócoli, G. Kasiri, F. La Mantia, Phase transformation of copper
- 26
- 27
- 28 hexacyanoferrate (KCuFe(CN)₆) during zinc insertion: Effect of co-ion
- 29
- 30
- 31 intercalation, *J. Power Sources.* 400 (2018) 167–171.
- 32
- 33 <https://doi.org/10.1016/j.jpowsour.2018.08.015>.
- 34
- 35
- 36 [27] J. Lim, G. Kasiri, R. Sahu, K. Schweinar, K. Hengge, D. Raabe, F. La Mantia,
- 37
- 38
- 39 C. Scheu, Irreversible Structural Changes of Copper Hexacyanoferrate Used as
- 40
- 41
- 42 a Cathode in Zn-Ion Batteries, *Chem. - A Eur. J.* 26 (2020) 4917–4922.
- 43
- 44 <https://doi.org/10.1002/chem.201905384>.
- 45
- 46
- 47 [28] V. Renman, D.O. Ojwang, M. Valvo, C.P. Gómez, T. Gustafsson, G. Svensson,
- 48
- 49
- 50
- 51 Structural-electrochemical relations in the aqueous copper
- 52
- 53
- 54 hexacyanoferrate-zinc system examined by synchrotron X-ray diffraction, *J.*
- 55
- 56
- 57 Power Sources. 369 (2017) 146–153.
- 58
- 59 <https://doi.org/10.1016/j.jpowsour.2017.09.079>.
- 60
- 61
- 62
- 63
- 64
- 65

- 1 [29] A. Mullaliu, J. Asenbauer, G. Aquilanti, S. Passerini, M. Giorgetti,
2
3 Highlighting the Reversible Manganese Electroactivity in Na-Rich Manganese
4
5 Hexacyanoferrate Material for Li- and Na-Ion Storage, *Small Methods*. 4
6
7
8
9 (2020). <https://doi.org/10.1002/smtd.201900529>.
10
- 11 [30] J.R. Plaisier, L. Nodari, L. Gigli, E.P.R.S. Miguel, R. Bertoncetto, A. Lausi,
12
13 The X-ray diffraction beamline MCX at Elettra: A case study of
14
15 non-destructive analysis on stained glass, *Acta IMEKO*. 6 (2017) 71–75.
16
17
18
19 https://doi.org/10.21014/acta_imeko.v6i3.464.
20
21
- 22 [31] J. Rodríguez-Carvajal, Recent advances in magnetic structure determination by
23
24 neutron powder diffraction, *Phys. B Phys. Condens. Matter*. 192 (1993) 55–69.
25
26
27
28 [https://doi.org/10.1016/0921-4526\(93\)90108-I](https://doi.org/10.1016/0921-4526(93)90108-I).
29
30
- 31 [32] G. Aquilanti, M. Giorgetti, R. Dominko, L. Stievano, I. Arčon, N. Novello, L.
32
33 Olivi, Operando characterization of batteries using x-ray absorption
34
35 spectroscopy: Advances at the beamline XAFS at synchrotron Elettra, *J. Phys.*
36
37
38
39
40
41 *D. Appl. Phys.* 50 (2017). <https://doi.org/10.1088/1361-6463/aa519a>.
42
- 43 [33] M. Newville, Data analysis for X-ray absorption spectroscopy using IFEFFIT
44
45 ATHENA , ARTEMIS , HEPHAESTUS : data analysis for X-ray absorption,
46
47
48 (2014). <https://doi.org/10.1107/S0909049505012719>.
49
- 50 [34] S.J. Gerber, E. Erasmus, Electronic effects of metal hexacyanoferrates : An
51
52 XPS and FTIR study, *Mater. Chem. Phys.* 203 (2018) 73–81.
53
54
55
56
57 <https://doi.org/10.1016/j.matchemphys.2017.09.029>.
58
- 59 [35] D.O. Ojwang, J. Grins, D. Wardecki, M. Valvo, V. Renman, T. Ericsson, T.
60
61
62
63
64
65

- 1 Gustafsson, A. Mahmoud, P. Hermann, G. Svensson, *Structure*
2
3 Characterization and Properties of K⁻ Containing Copper Hexacyanoferrate,
4
5
6 (2016). <https://doi.org/10.1021/acs.inorgchem.6b00227>.
7
8
9 [36] M.A. Oliver-Tolentino, J. Vázquez-Samperio, S.N. Arellano-Ahumada, A.
10
11 Guzmán-Vargas, D. Ramírez-Rosales, J.A. Wang, E. Reguera, Enhancement of
12
13 Stability by Positive Disruptive Effect on Mn-Fe Charge Transfer in
14
15 Vacancy-Free Mn-Co Hexacyanoferrate Through a Charge/Discharge Process
16
17 in Aqueous Na-Ion Batteries, *J. Phys. Chem. C.* 122 (2018) 20602–20610.
18
19
20
21
22 <https://doi.org/10.1021/acs.jpcc.8b05506>.
23
24
25 [37] M.H. Alfaruqi, V. Mathew, J. Gim, S. Kim, J. Song, J.P. Baboo, S.H. Choi, J.
26
27 Kim, Electrochemically induced structural transformation in a γ -MnO₂ cathode
28
29 of a high capacity zinc-ion battery system, *Chem. Mater.* 27 (2015) 3609–3620.
30
31
32
33 <https://doi.org/10.1021/cm504717p>.
34
35
36 [38] N. Zhang, F. Cheng, Y. Liu, Q. Zhao, K. Lei, C. Chen, X. Liu, J. Chen,
37
38 Cation-Deficient Spinel ZnMn₂O₄ Cathode in Zn(CF₃SO₃)₂ Electrolyte for
39
40 Rechargeable Aqueous Zn-Ion Battery, *J. Am. Chem. Soc.* 138 (2016)
41
42 12894–12901. <https://doi.org/10.1021/jacs.6b05958>.
43
44
45
46
47 [39] Q. Yang, F. Mo, Z. Liu, L. Ma, X. Li, D. Fang, S. Chen, S. Zhang, C. Zhi,
48
49 Activating C-Coordinated Iron of Iron Hexacyanoferrate for Zn Hybrid-Ion
50
51 Batteries with 10 000-Cycle Lifespan and Superior Rate Capability, *Adv.*
52
53 *Mater.* 31 (2019) 1–9. <https://doi.org/10.1002/adma.201901521>.
54
55
56
57
58 [40] M. Giorgetti, A Review on the Structural Studies of Batteries and Host
59
60
61
62
63
64
65

1 Materials by X-Ray Absorption Spectroscopy, 2013 (2013).

2
3 [41] E.Y.M. Lee, N. Tran, J. Russell, R.N. Lamb, Nanocrystalline order of zinc
4 oxide thin films grown on optical fibers, *J. Appl. Phys.* 92 (2002) 2996–2999.
5
6 <https://doi.org/10.1063/1.1495064>.
7
8

9
10 [42] J. Haug, A. Chassé, M. Dubiel, C. Eisenschmidt, M. Khalid, P. Esquinazi,
11
12 Characterization of lattice defects by x-ray absorption spectroscopy at the Zn
13
14 K-edge in ferromagnetic, pure ZnO films, *J. Appl. Phys.* 110 (2011).
15
16
17 <https://doi.org/10.1063/1.3631774>.
18
19

20 [43] Q. Yang, F. Mo, Z. Liu, L. Ma, X. Li, D. Fang, S. Chen, S. Zhang, C. Zhi,
21
22 Activating C-Coordinated Iron of Iron Hexacyanoferrate for Zn Hybrid-Ion
23
24 Batteries with 10 000-Cycle Lifespan and Superior Rate Capability, *Adv.*
25
26
27
28
29
30
31 *Mater.* 31 (2019) 0–17. <https://doi.org/10.1002/adma.201901521>.
32

33 [44] G. Ni, B. Han, Q. Li, Z. Ji, B. Huang, C. Zhou, Instability of Zinc
34
35 Hexacyanoferrate Electrode in an Aqueous Environment: Redox-Induced
36
37
38
39
40
41
42 Phase Transition, Compound Dissolution, and Inhibition, *ChemElectroChem.* 3
43
44
45
46
47
48
49
50
51
52
53
54
55
56
57
58
59
60
61
62
63
64
65
(2016) 798–804. <https://doi.org/10.1002/celc.201500538>.

August 8th, 2021

Editorial Office
Electrochimica Acta

A contribution to the Special Issue “*And Yet Electrochemical Energy Storage and Conversion Moves in 2021 - EESC 2021*”

Dear Editor,

Please find enclosed the following paper submitted for publication to *Electrochimica Acta* that is a contribution for the Special Issue “*And Yet Electrochemical Energy Storage and Conversion Moves in 2021 - EESC 2021*” of the journal “*Electrochimica Acta*” dedicated to the Workshop “First Italian Workshop on Energy Storage 2021 - IWES2021”. The manuscript is entitled “*Electrochemical performance of Manganese Hexacyanoferrate cathode material in aqueous Zn-ion battery*” and it is co-authored by Min Li, Rosalinda Sciacca, Mariam Maisuradze, Giuliana Aquilanti, Jasper Plaisier, Mario Berrettoni, and I. We feel that this paper is completely related to the contribution that I have given at the workshop and fully coherent with the topics covered during the Workshop.

I state that the work has not been published previously, is not under consideration for publication elsewhere, and is approved by all authors and host authorities.

A file concerning the Supplementary Information (SI) for publication has been enclosed as well.

A list of potential referees who are expert in the field are:

- 1 Prof. Edilso Reguera
National Polytechnic Institute of Mexico, CICATA-IPN
Email: edilso.reguera@gmail.com
(expert in hexacyanoferrates and battery materials)
- 2 Prof. Anne Bleuzen
Université Paris-Saclay
Email: anne.bleuzen@u-psud.fr
(expert in hexacyanoferrates)
- 3 Prof. Sylvain Cristol
University of Lille
Email: sylvain.cristol@univ-lille.fr
(expert in spectroscopy and diffraction)

Please direct all correspondence to my attention.

With Regards,

Marco Giorgetti
Associate Professor

Corresponding author's mailing address:

Prof. Marco Giorgetti

University of Bologna

Department of Industrial Chemistry "Toso Montanari"

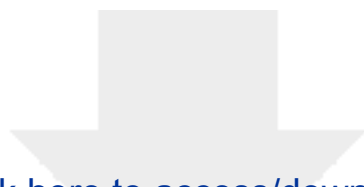
Viale del Risorgimento 4

I-40136 Bologna (BO), Italy

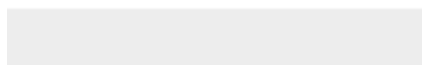
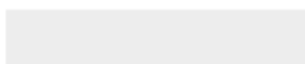
Ph: +39 051 209 3666. fax: +39 051 209 3666. email: marco.giorgetti@unibo.it

HIGHLIGHTS

- Sodium manganese hexacyanoferrate show high specific capacity in aqueous Zn-ion battery
- Fe-site was activated at beginning cycles owing to the dissolution of Mn-site
- Zn-ions inserted to the Mn-site during cycling and forming Zn-N-C-Fe structure
- XAS data indicate the Fe electro-activity



Click here to access/download
Supplementary Materials
080621-zinc-ion battery_si.docx



August 8th, 2021

With reference to our paper being submitted to *Electrochimica Acta* entitled “*Electrochemical performance of Manganese Hexacyanoferrate cathode material in aqueous Zn-ion battery*” and it is co-authored by Min Li, Rosalinda Sciacca, Mariam Maisuradze, Giuliana Aquilanti, Jasper Plaisier, Mario Berrettoni, and I, which has been submitted to *Electrochimica Acta*,

I declare that this is a contribution for the Special Issue “*And Yet Electrochemical Energy Storage and Conversion Moves in 2021 - EESC 2021*” dedicated to the Workshop “First Italian Workshop on Energy Storage 2021 - IWES2021”. The topic/issue covered in the paper are completely related to the contribution that I have given at the workshop and fully coherent with the topics covered during the Workshop.

I am also stating that the work described has not been published previously, that it is not under consideration for publication elsewhere, that its publication is approved by all authors and tacitly or explicitly by the responsible authorities where the work was carried out, and that, if accepted, it will not be published elsewhere in the same form, in English or in any other language, including electronically without the written consent of the copyright holder.

With Regards,

Marco Giorgetti
Associate Professor

Corresponding author's mailing address:

Prof. Marco Giorgetti

University of Bologna

Department of Industrial Chemistry "Toso Montanari"

Viale del Risorgimento 4

I-40136 Bologna (BO), Italy

Ph: +39 051 209 3666. fax: +39 051 209 3666. email: marco.giorgetti@unibo.it